

# Convective Excitation of Inertial Modes in Binary Neutron Star Mergers

Roberto De Pietri,<sup>1,2</sup> Alessandra Feo,<sup>3,2</sup> José A. Font,<sup>4,5</sup> Frank Löffler,<sup>6,7</sup>  
Francesco Maione,<sup>1,2</sup> Michele Pasquali,<sup>1,2</sup> and Nikolaos Stergioulas<sup>8</sup>

<sup>1</sup>*Parma University, Parco Area delle Scienze 7/A, I-43124 Parma (PR), Italy*

<sup>2</sup>*INFN gruppo collegato di Parma, Parco Area delle Scienze 7/A, I-43124 Parma (PR), Italy*

<sup>3</sup>*Department of Chemistry, Life Sciences and Environmental Sustainability,  
Parma University, Parco Area delle Scienze, 157/A, I-43124 Parma (PR), Italy*

<sup>4</sup>*Departamento de Astronomía y Astrofísica, Universitat de València,*

*Dr. Moliner 50, 46100, Burjassot (València), Spain*

<sup>5</sup>*Observatori Astronòmic, Universitat de València,*

*C/ Catedrático José Beltrán 2, 46980, Paterna (València), Spain*

<sup>6</sup>*Heinz-Nixdorf Chair for Distributed Information Systems,*

*Friedrich Schiller University Jena, 07443 Jena, Germany*

<sup>7</sup>*Center for Computation & Technology, Louisiana State University, Baton Rouge, LA 70803 USA*

<sup>8</sup>*Department of Physics, Aristotle University of Thessaloniki, Thessaloniki 54124, Greece*

(Dated: July 4, 2018)

We present the first very long-term simulations (extending up to  $\sim 140$  ms after merger) of binary neutron star mergers with piecewise polytropic equations of state and in full general relativity. Our simulations reveal that at a time of 30-50 ms after merger, parts of the star become convectively unstable, which triggers the excitation of inertial modes. The excited inertial modes are sustained up to several tens of milliseconds and are potentially observable by the planned third-generation gravitational-wave detectors at frequencies of a few kilohertz. Since inertial modes depend on the rotation rate of the star and they are triggered by a convective instability in the postmerger remnant, their detection in gravitational waves will provide a unique opportunity to probe the rotational and thermal state of the merger remnant. In addition, our findings have implications for the long-term evolution and stability of binary neutron star remnants.

PACS numbers: 04.25.D-, 04.40.Dg, 95.30.Lz, 97.60.Jd

*Introduction.*— On August 17, 2017, the Advanced LIGO and Advanced Virgo detectors observed the first gravitational-wave (GW) signal produced by the merger of two neutron stars in a binary system, GW170817 [1]. This landmark detection initiated the field of GW multimessenger astronomy [2] in which, thanks to the unprecedented coordinated action of LIGO, Virgo and some 70 astronomical facilities, both ground-based and in space, key evidence to address open issues in relativistic astrophysics was collected. GW170817 has probed the origin of short gamma-ray bursts [3] and kilonovae and the  $r$ -process-mediated nucleosynthesis of heavy elements [4], along with providing independent measures of cosmological parameters [5].

Numerical relativity simulations of binary neutron star (BNS) mergers have shown that the outcome depends primarily on the masses of the individual stars and on the equation of state (EOS) (see [6–9] for recent reviews). Prompt collapse to a black hole happens above a certain threshold mass, while delayed collapse or no collapse is produced otherwise. In the latter cases, the remnant is a hypermassive (HMNS) [10] or supramassive neutron star [11], respectively. Simulations of their postmerger phase, lasting up to a few tens of milliseconds, show the emission of significant amounts of gravitational radiation at distinct frequencies of a few kilohertz (e.g. [12–30]), with contributions as low as  $\sim 1$  kHz, depending on the

EOS [31].

It was first shown in Ref. [19], through a mode analysis, that in many cases the postmerger emission includes, apart from a dominant  $m = 2$   $f$ -mode (denoted as  $f_2$  or  $f_{\text{peak}}$ ), secondary, quasilinear combination frequencies between the  $f$ -mode and the quasiradial,  $m = 0$  mode (sums and differences, denoted as  $f_{2-0}$  and  $f_{2+0}$ , respectively). These frequencies thus form an equidistant triplet. The combination frequencies are primarily present in soft EOS models with high mass [24]. In addition, in [24] it was found that in stiff EOS models with low mass a different secondary peak,  $f_{\text{spiral}}$ , due to a spiral deformation excited during merger, can have comparable or larger amplitude than  $f_{2-0}$  and a frequency systematically larger than  $f_{2-0}$ . The detection of GWs in the postmerger remnant can lead to tight constraints on the neutron star EOS, primarily through the application of an empirical relation between the  $m = 2$   $f$ -mode frequency and the neutron star radius [20, 21, 24, 32–37] (see [38] for the first search of postmerger GWs in GW170817). For additional studies of the properties of postmerger remnants, see e.g. [31, 39–48].

In previous simulations, the dynamics of the remnant was followed up to  $\sim 40$  ms after the merger. In this *Letter* we present the first very long-term simulations of BNS mergers (reaching up to  $\sim 140$  ms after merger) using a piecewise polytropic EOS with a thermal part. Our sim-

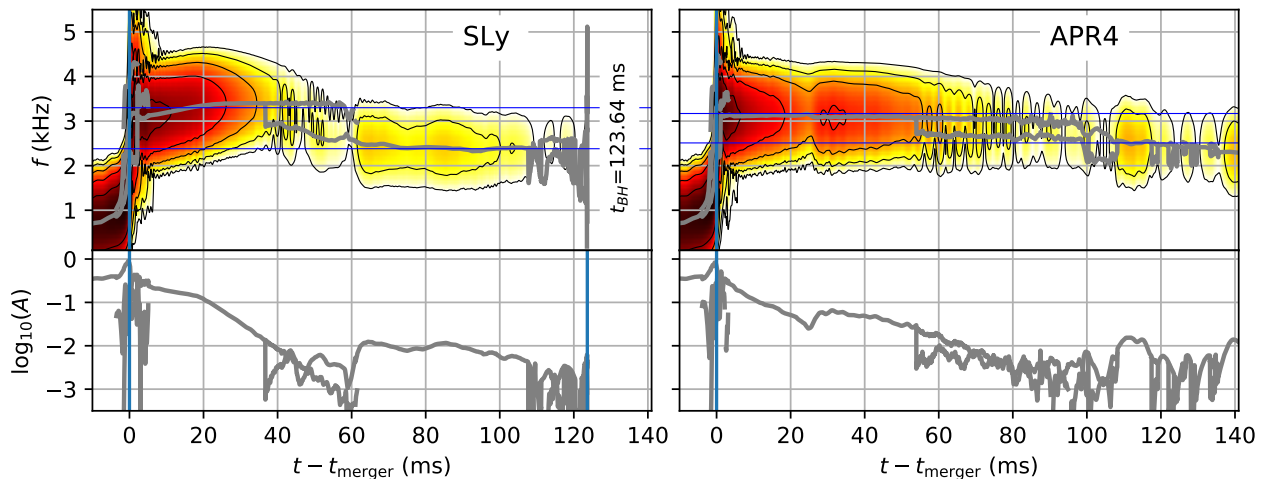


FIG. 1. Top panels: time-frequency spectrograms of the  $h_{22}$  component of the GW signals for both EOS. The thick gray lines indicate the frequency of the active spectral mode responsible for the GW emission. Colors indicate the relative intensity of the spectral density (darker areas correspond to higher intensity). Bottom panels: mode amplitudes (in arbitrary units).

ulations reveal that at  $t - t_{\text{merger}} \sim 30 - 50$  ms (depending on the model), the initial  $m = 2$   $f$ -mode oscillation has diminished and parts of the star become convectively unstable. Subsequently, the convective instability triggers the excitation of global, discrete inertial modes, in which the Coriolis force is the dominant restoring force. The inertial modes are sustained up to several tens of ms and will be detectable by the planned third-generation GW detectors at frequencies of a few kHz. We note that these are the first simulations of BNS mergers that show the excitation of inertial modes.

Detailed perturbative studies will be required to identify the particular inertial modes excited in BNS mergers, which could be either polar-led (gravito-inertial) or axial-led (similar to  $r$ -modes); see [49] for definitions. Since inertial-mode frequencies depend on the rotation rate of the star and their existence in the postmerger phase is triggered by a convective instability, their detection in GWs will provide a unique opportunity to probe the rotational and thermal state of the merger remnant. Our findings also have implications for the long-term evolution and stability of BNS remnants.

*Initial data and methods.*— Initial data were generated with the LORENE code [50, 51]. We employ two EOS, namely the APR4 and SLy EOS, parametrized as piecewise polytropes [52] with 7 pieces plus a thermal component with adiabatic index  $\Gamma_{\text{th}} = 1.8$ . We consider systems of total mass of  $2.56 M_{\odot}$ , with an initial separation of roughly 44.3 km (four full orbits before merger) and an initial angular velocity of  $\simeq 1770 \text{ s}^{-1}$ . In particular, we consider equal-mass systems characterized by relatively low-mass components, below the range of the inferred masses for GW170817 [1] (total mass between 2.73 and  $3.29 M_{\odot}$  for conservative spin priors). The compactness of the stars is 0.166 for the APR4 EOS and 0.161 for the SLy EOS. The remnant HMNS survives for more than

100 ms before collapsing to a black hole, developing interesting new dynamics, as we show below. The simulations were performed using the Einstein Toolkit [53] employing the same setting of [31, 43, 54, 55]. The only difference is the use of  $\pi$ -symmetry to reduce the computational cost by a factor of 2 (but one model was also compared to a simulation without  $\pi$ -symmetry). This allowed us to extend the limit of the simulation time up to  $\sim 160$  ms, of which the last 140 ms correspond to the postmerger phase. The reported simulations employed a finest resolution of  $\Delta x \simeq 275$  m. The outermost grid boundary was set at  $\sim 1040$  km from the center of mass of the system. Despite the long evolution times of our simulations, the numerical violations of the Hamiltonian and momentum constraints converge away at the expected 2nd order upon increasing the grid resolution. Convergence, as well as the overall behavior of the evolutions and the appearance of convective instabilities and different modes at specific times, has been checked by performing additional simulations employing grid resolutions of  $\Delta x = 369$  m and  $\Delta x = 185$  m (at the innermost refinement level) for selected models. Details will be reported in [56].

*Results overview.*—The general dynamics of our BNS mergers is summarized in Figure 1 for both EOS. The upper panels show time-frequency spectrograms of the  $h_{22}$  component of the spherical-harmonic decomposition of the GW signals. We superimpose the frequency (thick gray lines) of the dominant spectral modes which we determine using the ESPRIT Prony’s method (using a moving window interval of 3 ms) as discussed in [31]. In the lower panels, we show the time evolution of the corresponding extracted amplitudes (in arbitrary units). For the SLy EOS, the postmerger remnant survives for over 120 ms before collapsing to a black hole. For the APR4 EOS, the remnant has not collapsed even after 140 ms.

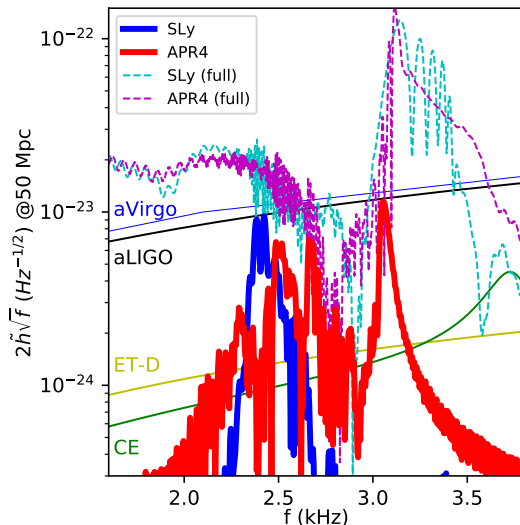


FIG. 2. GW spectrum for a BNS merger at 50 Mpc at the optimal orientation. It is shown for the entire GW signal (dashed lines) and for a restricted time window (see main text) where inertial modes are active (solid lines). The design sensitivities of Advanced Virgo [57], Advanced LIGO [58], Einstein Telescope [59], and Cosmic Explorer [60] are shown for reference.

The dominant mode in the *early* postmerger phase is the  $m = 2$   $f$ -mode, with a frequency above 3 kHz for both EOS and a decaying amplitude. However, we find that a *distinct*, lower-frequency mode appears later in the evolution, at  $t - t_{\text{merger}} \sim 35$  ms for SLy and  $\sim 55$  ms for APR4. At later times, the new mode becomes the dominant emitter of GWs.

The mode dynamics is imprinted in the GW signal, whose spectrum is displayed in Fig. 2. We show the PSD of the GW signal for a maximally-aligned source at a distance of 50 Mpc, both for the whole simulation (dashed lines), and restricted to the interval between 55 ms and 140 ms after the merger (solid lines). In the former case, GW emission dominates the spectrum between 3 kHz and 3.5 kHz for the SLy EOS, and shows a single higher peak at 3.17 kHz for the APR4 EOS. On the other hand, when selecting the signal in the range between 55 ms and 140 ms, the spectrum is dominated by a peak at frequency 2.38 kHz in the case of the SLy EOS while we see different peaks at frequencies of  $\sim 2.3$  kHz,  $\sim 2.5$  kHz  $\sim 2.7$  kHz for the APR4 EOS, corresponding to inertial modes excited at different times. We note that there is sufficient power in these lower-frequency modes to render them potentially observable by third-generation detectors. For a source at 50 Mpc the expected Cosmic Explorer [60] S/N ratio for optimal use of matched filtering techniques for the signal emitted between 55 ms up to 140 ms after merger are  $\sim 3.5$  and  $\sim 3.7$  for SLy and APR4 EOS, respectively (for the Einstein Telescope-D [59] they are  $\sim 2.5$  and  $\sim 2.9$  but enhancement can be expected due

to the triangular arrangement with three non-aligned interferometers, see [37]). A first insight into the nature of this late-time feature can be obtained by examining the eigenfunction of the mode, which we extract by taking the FFT of the time series of the rest-mass density in the equatorial plane and plotting the amplitude at a specific frequency (see [61]). The first row of Figure 3 shows the eigenfunction of the dominant  $m = 2$   $f$ -mode at an early time, for the two models. These eigenfunctions have no azimuthal nodal line, corresponding to a fundamental mode. The last panel in the upper row of Figure 3 shows the extracted eigenfunction for the SLy model in the vertical plane, which is consistent with an  $m = 2$   $f$ -mode [62].

The second row of Figure 3 shows the eigenfunction of the distinct, lower-frequency modes at a late time, for the two models. The eigenfunctions still have an  $m = 2$  character in the equatorial plane, but there are also azimuthal nodal lines, which is a characteristic of modes with higher radial order. In addition, the amplitude vanishes in the core and peaks at the outer layers of the remnant. The last panel in the lower row in Fig. 3 shows the extracted eigenfunction for the SLy model in the vertical plane, which is consistent with an inertial mode [63].

*Convective stability and inertial modes.*—The late-time, lower-frequency modes found in our simulations can be interpreted as inertial modes, for which the Coriolis force is the dominant restoring force. The growth of the inertial modes (up to their saturation amplitude) is triggered by a convective instability that appears in the nonisentropic remnant shortly before the inertial modes start to grow from a small amplitude.

The local convective instability depends on the sign of the Schwarzschild discriminant

$$A_\alpha = \frac{1}{\varepsilon + p} \nabla_\alpha \varepsilon - \frac{1}{\Gamma_1 p} \nabla_\alpha p, \quad (1)$$

where  $\Gamma_1 := (\varepsilon + p)/p(dp/d\varepsilon)_s = (d \ln p/d \ln \rho)_s$  is the adiabatic index of linear perturbations about a pseudo-barotropic equilibrium (see [62] and references therein) and where  $\varepsilon$  is the energy density. Regions with  $A_\alpha < 0$  are convectively stable, whereas regions with  $A_\alpha > 0$  are convectively *unstable*. For a piecewise polytropic EOS we calculate  $\Gamma_1$  as

$$\Gamma_1 = \Gamma_{\text{th}} + (\Gamma_i - \Gamma_{\text{th}}) \frac{K_i \rho^{\Gamma_i}}{p}, \quad (2)$$

where  $K_i$  and  $\Gamma_i$  are the polytropic constant and exponent in the  $i$ -th piece of the EOS, respectively, and  $\Gamma_{\text{th}}$  is the adiabatic index of the added thermal part. To determine the convective stability in the star, we evaluate  $A_r$  and  $A_\theta$  in the equatorial and vertical planes, at different times during the evolution.

Figure 4 shows the convectively unstable regions, where  $A_r > 0$  (dark color), in the equatorial plane for the SLy model. The top left panel shows an instant at

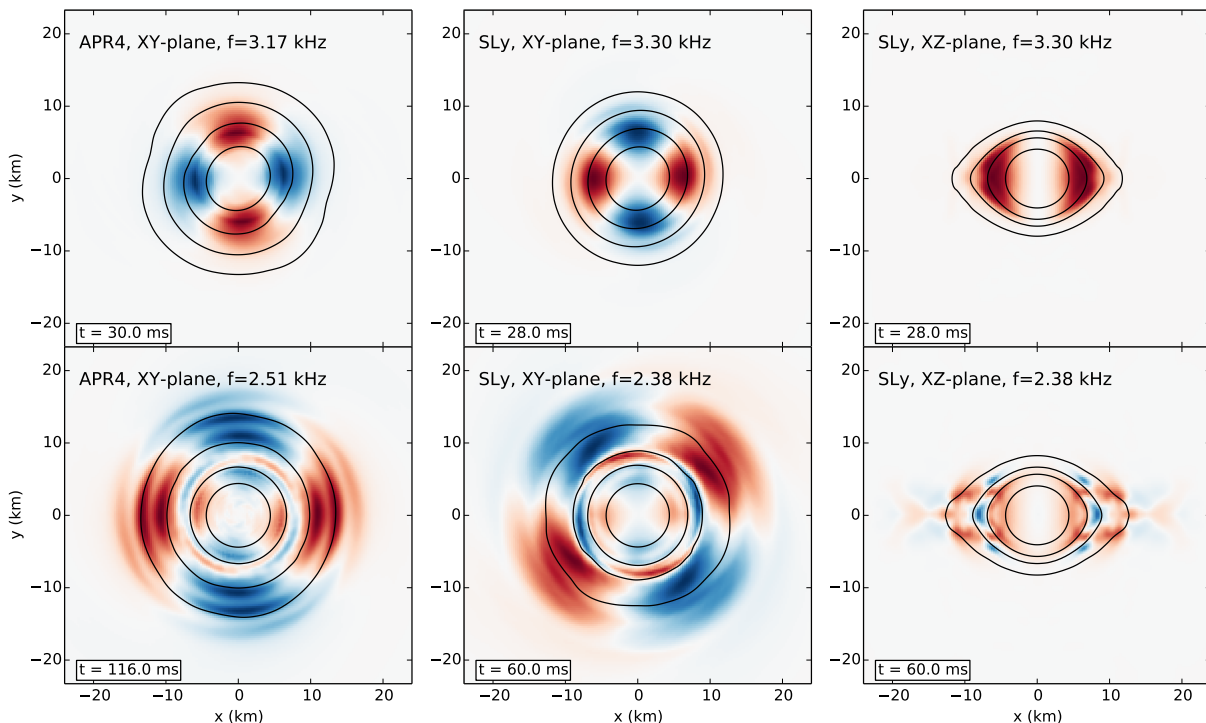


FIG. 3. Left and center panels: density eigenfunctions in the equatorial plane for particular modes at different times (relative to the merger time), for the two models considered. Right panel: the corresponding eigenfunctions in the vertical plane for the SLy model. The black lines are isocontours of the rest-mass density with values (for decreasing radii)  $1.5 \times 10^{13}$ ,  $8 \times 10^{13}$ ,  $3 \times 10^{14}$ , and  $8 \times 10^{14}$  ( $\text{g}/\text{cm}^3$ ).

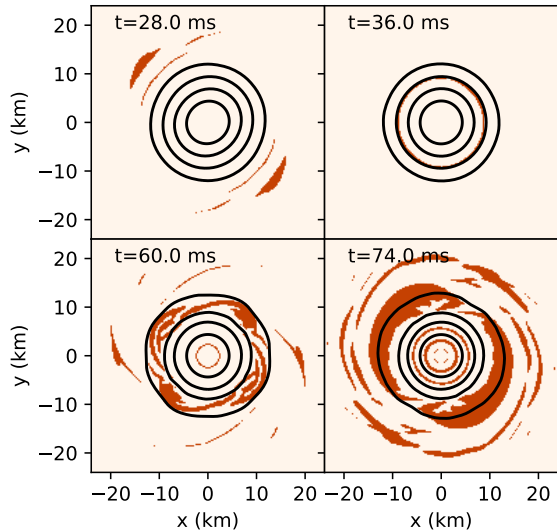


FIG. 4. Snapshots of  $A_r$  in the equatorial plane for the SLy model at different times relative to the merger time. Convectively unstable regions are shown with dark color.

an early time ( $t = 28$  ms), when most of the star (except for some parts in the low-density envelope) is convectively stable and the  $m = 2$   $f$ -mode dominates the GW spectrum. The entropy in the remnant created by shock heating during merger (not shown here) is concentrated in an expanding envelope around a relatively cold

core (two initial hot spots mix into a nearly axisymmetric structure in the early postmerger phase, as also found by [44]).

At  $t = 36$  ms, a convectively unstable ring appears in the equatorial plane, at  $\rho \simeq 8 \times 10^{13} \text{g}/\text{cm}^3$ . This coincides with the first appearance of inertial modes in Fig. 1. In accordance with the observed growth of convective motions, at  $t = 60$  ms, the first convectively unstable ring has expanded to lower densities and appears fragmented, which coincides with a strong growth of an inertial mode with frequency of 2.38 kHz in Fig. 1. The amplitude of the inertial mode only diminishes slightly for the next 15 ms. At  $t = 74$  ms, the convectively unstable regions have expanded further and we observe a renewed growth of the amplitude of the inertial mode in Fig. 1. We thus observe a strong correlation between the appearance of several convectively unstable regions in the remnant and the appearance and growth of inertial modes.

Inertial modes can be either polar-led (gravito-inertial modes) or axial-led ( $r$ -mode like). In slowly-rotating stars, gravito-inertial modes become  $g$ -modes and we estimate a Brunt-Väissälä frequency  $\langle N \rangle / (2\pi) = 356 \text{Hz}$  using  $\Gamma = 1.36$ ,  $\Gamma_1 = 1.74$  and  $\rho = 8 \times 10^{13} \text{g}/\text{cm}^3$  (see [64]). These modes are also excited in protoneutron stars, in the context of core-collapse supernovae (see e.g. [65] and references therein). However, in rapidly rotating stars, gravito-inertial modes have very similar

properties to axial-led inertial modes, with frequencies being nearly proportional to the rotational frequency of the star [64, 66, 67]. The  $m = 2$  inertial modes identified in the simulations of the two models discussed here have frequencies only somewhat smaller than twice the maximum angular frequency in the differentially rotating star  $\Omega_{\max}$  whose rotational profile is consistent with results found in [47, 68] that will be reported in [56] (notice that the  $m = 2$   $f$ -mode frequency appearing at early times has been empirically associated with  $2\Omega_{\max}$  [42]). The characterization of the (polar- or axial-led) inertial modes that are excited in our simulations can be achieved after a comparison with detailed perturbative studies, which we plan to undertake in the future. We finally note that mergers with unequal mass components may also show the excitation of odd modes, which are suppressed in our present equal-mass simulations with  $\pi$ -symmetry. For the evolution of models very close to the ones discussed here, neutrino effects have been considered in [48], while the timescales for magnetic effects and the MRI-induced effective viscosity have been analyzed in detail in [69]. These effects should be reconsidered on long timescales of up to 140 ms.

*Conclusions.*—The appearance of convectively unstable regions and the excitation of particular inertial modes in long-lived remnants of BNS mergers depends on the rotational and thermal state of the remnant and impacts its dynamical evolution. Whereas, in this first investigation, we considered a piecewise polytropic EOS with a thermal component (that has the advantage of having a well-defined, analytically expressed thermodynamics) and we ignored the dependence on composition gradients, magnetic fields and neutrino transport (which should be clearly investigated in future simulations), our results imply that either the presence or the absence of inertial modes in the late-time GW spectrum of BNS mergers will be a sensitive probe of neutron star physics.

We are grateful to Nils Andersson, Andreas Bauswein, James Alexander Clark, Roland Haas and John Friedman for comments on the manuscript. We thank the many developers of the public software used for this research, namely LORENE and the Einstein Toolkit. Computational resources were provided by PRACE Grant No. Pra14\_3593, by the CINECA-INFN agreement, by the Louisiana Optical Network Initiative (QB2, allocations loni\_hyrel, loni\_numrel, and loni\_cactus), by the LSU HPC facilities (SuperMic, allocation hpc\_hyrel) and by the GWAVES (pr002022) allocation on the ARIS facility of GRNET in Athens. JAF is supported by the Spanish MINECO (AYA2015-66899-C2-1-P), by the Generalitat Valenciana (PROMETEOII-2014-069), and by the H2020-MSCA-RISE-2017 Grant No. FunFiCO-777740. FL was supported by the NSF in the USA as part of the Einstein Toolkit (Grants No. 1550551, No. 1550461, No. 1550436, No. 1550514). Support by

the COST Actions MP1304 (NewCompStar), CA16104 (GWVerse) and CA16214 (PHAROS) is kindly acknowledged.

- 
- [1] B. P. Abbott, R. Abbott, T. D. Abbott, F. Acernese, K. Ackley, C. Adams, T. Adams, P. Addesso, R. X. Adhikari, V. B. Adya, and et al., *Phys. Rev. Lett.* **119**, 161101 (2017), arXiv:1710.05832 [gr-qc].
  - [2] B. P. Abbott, R. Abbott, T. D. Abbott, F. Acernese, K. Ackley, C. Adams, T. Adams, P. Addesso, R. X. Adhikari, V. B. Adya, and et al., *Astrophysics J.* **848**, L12 (2017), arXiv:1710.05833 [astro-ph.HE].
  - [3] B. P. Abbott *et al.* (Virgo, Fermi-GBM, INTEGRAL, LIGO Scientific), *Astrophys. J.* **848**, L13 (2017), arXiv:1710.05834 [astro-ph.HE].
  - [4] B. P. Abbott *et al.* (Virgo, LIGO Scientific), *Astrophys. J.* **850**, L39 (2017), arXiv:1710.05836 [astro-ph.HE].
  - [5] B. P. Abbott *et al.* (LIGO Scientific, VIRGOUE, Las Cumbres Observatory, DES, DLT40, Virgo, 1M2H, Dark Energy Camera GW-E, MASTER), *Nature* **551**, 85 (2017), arXiv:1710.05835 [astro-ph.CO].
  - [6] M. D. Duez, *Class. and Quant. Grav.* **27**, 114002 (2010), arXiv:0912.3529 [astro-ph.HE].
  - [7] J. A. Faber and F. A. Rasio, *Liv. Rev. Rel.* **15**, 8 (2012), arXiv:1204.3858 [gr-qc].
  - [8] V. Paschalidis, *Class. Quant. Grav.* **34**, 084002 (2017), arXiv:1611.01519 [astro-ph.HE].
  - [9] L. Baiotti and L. Rezzolla, *Rep. Prog. Phys.* **80**, 096901 (2017), arXiv:1607.03540 [gr-qc].
  - [10] T. W. Baumgarte, S. L. Shapiro, and M. Shibata, *Astrophys. J.* **528**, L29 (2000), arXiv:astro-ph/9910565 [astro-ph].
  - [11] G. Cook, S. Shapiro, and S. Teukolsky, *Astrophys. J.* **398**, 203 (1992).
  - [12] X. Zhuge, J. M. Centrella, and S. L. W. McMillan, *Phys. Rev. D* **50**, 6247 (1994).
  - [13] M. Shibata and K. b. o. Uryū, *Phys. Rev. D* **61**, 064001 (2000).
  - [14] R. Oechslin, S. Rosswog, and F.-K. Thielemann, *Phys. Rev. D* **65**, 103005 (2002), gr-qc/0111005.
  - [15] M. Shibata and K. Uryū, *Progress of Theoretical Physics* **107**, 265 (2002), gr-qc/0203037.
  - [16] M. Shibata, K. Taniguchi, and K. Uryū, *Phys. Rev. D* **71**, 084021 (2005), gr-qc/0503119.
  - [17] M. Shibata and K. Taniguchi, *Phys. Rev. D* **73**, 064027 (2006), astro-ph/0603145.
  - [18] K. Kiuchi, Y. Sekiguchi, M. Shibata, and K. Taniguchi, *Phys. Rev. D* **80**, 064037 (2009), arXiv:0904.4551 [gr-qc].
  - [19] N. Stergioulas, A. Bauswein, K. Zagkouris, and H.-T. Janka, *Mon. Not. Roy. Astron. Soc.* **418**, 427 (2011), arXiv:1105.0368 [gr-qc].
  - [20] A. Bauswein and H. T. Janka, *Phys. Rev. Lett.* **108**, 011101 (2012), arXiv:1106.1616 [astro-ph.SR].
  - [21] A. Bauswein, H. T. Janka, K. Hebeler, and A. Schwenk, *Phys. Rev.* **D86**, 063001 (2012), arXiv:1204.1888 [astro-ph.SR].
  - [22] K. Hotokezaka, K. Kiuchi, K. Kyutoku, T. Muranushi, Y.-i. Sekiguchi, M. Shibata, and K. Taniguchi, *Phys. Rev.* **D88**, 044026 (2013), arXiv:1307.5888 [astro-ph.HE].

- [23] K. Takami, L. Rezzolla, and L. Baiotti, *Phys. Rev.* **D91**, 064001 (2015), arXiv:1412.3240 [gr-qc].
- [24] A. Bauswein and N. Stergioulas, *Phys. Rev.* **D91**, 124056 (2015), arXiv:1502.03176 [astro-ph.SR].
- [25] S. Bernuzzi, T. Dietrich, and A. Nagar, *Phys. Rev. Lett.* **115**, 091101 (2015), arXiv:1504.01764 [gr-qc].
- [26] T. Dietrich, S. Bernuzzi, M. Ujevic, and B. Brügmann, *Phys. Rev.* **D91**, 124041 (2015), arXiv:1504.01266 [gr-qc].
- [27] T. Dietrich, S. Bernuzzi, M. Ujevic, and W. Tichy, (2016), arXiv:1611.07367 [gr-qc].
- [28] T. Dietrich, M. Ujevic, W. Tichy, S. Bernuzzi, and B. Bruegmann, *Phys. Rev.* **D95**, 024029 (2017), arXiv:1607.06636 [gr-qc].
- [29] L. Rezzolla and K. Takami, *Phys. Rev.* **D93**, 124051 (2016), arXiv:1604.00246 [gr-qc].
- [30] L. Lehner, S. L. Liebling, C. Palenzuela, O. L. Caballero, E. O'Connor, M. Anderson, and D. Neilsen, *ArXiv e-prints* (2016), arXiv:1603.00501 [gr-qc].
- [31] F. Maione, R. De Pietri, A. Feo, and F. Löffler, *Phys. Rev.* **D96**, 063011 (2017), arXiv:1707.03368 [gr-qc].
- [32] J. Clark, A. Bauswein, L. Cadonati, H. T. Janka, C. Pankow, and N. Stergioulas, *Phys. Rev.* **D90**, 062004 (2014), arXiv:1406.5444 [astro-ph.HE].
- [33] J. A. Clark, A. Bauswein, N. Stergioulas, and D. Shoemaker, *Class. Quant. Grav.* **33**, 085003 (2016), arXiv:1509.08522 [astro-ph.HE].
- [34] A. Bauswein, N. Stergioulas, and H.-T. Janka, *Eur. Phys. J. A* **52**, 56 (2016), arXiv:1508.05493 [astro-ph.HE].
- [35] K. Chatziioannou, J. A. Clark, A. Bauswein, M. Millhouse, T. B. Littenberg, and N. Cornish, *ArXiv e-prints* (2017), arXiv:1711.00040 [gr-qc].
- [36] S. Bose, K. Chakravarti, L. Rezzolla, B. S. Sathyaprakash, and K. Takami, (2017), arXiv:1705.10850 [gr-qc].
- [37] H. Yang, V. Paschalidis, K. Yagi, L. Lehner, F. Pretorius, and N. Yunes, (2017), arXiv:1707.00207 [gr-qc].
- [38] B. P. Abbott, R. Abbott, T. D. Abbott, F. Acernese, K. Ackley, C. Adams, T. Adams, P. Addesso, R. X. Adhikari, V. B. Adya, and et al., *Astrophysical Journal Letters* **851**, L16 (2017), arXiv:1710.09320 [astro-ph.HE].
- [39] L. Baiotti, B. Giacomazzo, and L. Rezzolla, *Phys. Rev. D* **78**, 084033 (2008), arXiv:0804.0594 [gr-qc].
- [40] M. Anderson, E. W. Hirschmann, L. Lehner, S. L. Liebling, P. M. Motl, D. Neilsen, C. Palenzuela, and J. E. Tohline, *Phys. Rev. D* **77**, 024006 (2008), arXiv:0708.2720 [gr-qc].
- [41] Y. T. Liu, S. L. Shapiro, Z. B. Etienne, and K. Taniguchi, *Phys. Rev. D* **78**, 024012 (2008), arXiv:0803.4193.
- [42] W. Kastaun and F. Galeazzi, *Phys. Rev.* **D91**, 064027 (2015), arXiv:1411.7975 [gr-qc].
- [43] R. De Pietri, A. Feo, F. Maione, and F. Löffler, *Phys. Rev.* **D93**, 064047 (2016), arXiv:1509.08804 [gr-qc].
- [44] W. Kastaun, R. Ciolfi, and B. Giacomazzo, *Phys. Rev.* **D94**, 044060 (2016), arXiv:1607.02186 [astro-ph.HE].
- [45] V. Paschalidis, W. E. East, F. Pretorius, and S. L. Shapiro, *Phys. Rev. D* **92**, 121502 (2015), arXiv:1510.03432 [astro-ph.HE].
- [46] W. E. East, V. Paschalidis, and F. Pretorius, *ArXiv e-prints* (2016), arXiv:1609.00725 [astro-ph.HE].
- [47] M. Hanauske, K. Takami, L. Bovard, L. Rezzolla, J. A. Font, F. Galeazzi, and H. Stocker, *Phys. Rev.* **D96**, 043004 (2017), arXiv:1611.07152 [gr-qc].
- [48] F. Foucart, R. Haas, M. D. Duez, E. O'Connor, C. D. Ott, L. Roberts, L. E. Kidder, J. Lippuner, H. P. Pfeiffer, and M. A. Scheel, *Phys. Rev.* **D93**, 044019 (2016), arXiv:1510.06398 [astro-ph.HE].
- [49] J. L. Friedman and K. H. Lockitch, *Prog. Theor. Phys. Suppl.* **136**, 121 (1999), gr-qc/9908083.
- [50] LORENE, "LORENE: Langage Objet pour la RElativité NumériquE," <http://www.lorene.obspm.fr/>.
- [51] E.ourgoulhon, P. Grandclement, K. Taniguchi, J.-A. Marck, and S. Bonazzola, *Phys. Rev. D* **63**, 064029 (2001), arXiv:gr-qc/0007028.
- [52] J. S. Read, B. D. Lackey, B. J. Owen, and J. L. Friedman, *Phys. Rev.* **D79**, 124032 (2009).
- [53] F. Löffler, J. Faber, E. Bentivegna, T. Bode, P. Diener, R. Haas, I. Hinder, B. C. Mundim, C. D. Ott, E. Schnetter, G. Allen, M. Campanelli, and P. Laguna, *Class. Quant. Grav.* **29**, 115001 (2012), arXiv:1111.3344 [gr-qc].
- [54] F. Maione, R. De Pietri, A. Feo, and F. Löffler, *Class. Quant. Grav.* **33**, 175009 (2016), arXiv:1605.03424 [gr-qc].
- [55] A. Feo, R. De Pietri, F. Maione, and F. Löffler, *Class. Quant. Grav.* **34**, 034001 (2017), arXiv:1608.02810 [gr-qc].
- [56] R. De Pietri and et al, in preparation (2018).
- [57] F. Acernese *et al.* (VIRGO), *Class. Quant. Grav.* **32**, 024001 (2015), arXiv:1408.3978 [gr-qc].
- [58] J. Aasi *et al.* (LIGO Scientific), *Class. Quant. Grav.* **32**, 074001 (2015), arXiv:1411.4547 [gr-qc].
- [59] M. Punturo *et al.*, *Proceedings, 14th Workshop on Gravitational wave data analysis (GWDAW-14): Rome, Italy, January 26-29, 2010*, *Class. Quant. Grav.* **27**, 194002 (2010).
- [60] B. P. Abbott *et al.* (LIGO Scientific), *Class. Quant. Grav.* **34**, 044001 (2017), arXiv:1607.08697 [astro-ph.IM].
- [61] N. Stergioulas, T. A. Apostolatos, and J. A. Font, *Mon. Not. Roy. Astron. Soc.* **352**, 1089 (2004), astro-ph/0312648.
- [62] J. L. Friedman and N. Stergioulas, *Rotating Relativistic Stars* (Cambridge University Press, 2013).
- [63] W. Kastaun, *Phys. Rev. D* **77**, 124019 (2008), arXiv:0804.1151.
- [64] A. Passamonti, B. Haskell, N. Andersson, D. I. Jones, and I. Hawke, *Mon. Not. Roy. Astron. Soc.* **394**, 730 (2009), arXiv:0807.3457.
- [65] A. Torres-Forné, P. Cerdá-Durán, A. Passamonti, and J. A. Font, *Mon. Not. Roy. Astron. Soc.* **474**, 5272 (2018), arXiv:1708.01920 [astro-ph.SR].
- [66] K. H. Lockitch, N. Andersson, and J. L. Friedman, *Phys. Rev.* , 024019 (2001), gr-qc/0008019.
- [67] E. Gaertig and K. D. Kokkotas, *Phys. Rev. D* **80**, 064026 (2009), arXiv:0905.0821 [astro-ph.SR].
- [68] R. Ciolfi, W. Kastaun, B. Giacomazzo, A. Endrizzi, D. M. Siegel, and R. Perna, *Phys. Rev.* **D95**, 063016 (2017), arXiv:1701.08738 [astro-ph.HE].
- [69] K. Kiuchi, K. Kyutoku, Y. Sekiguchi, and M. Shibata, (2017), arXiv:1710.01311 [astro-ph.HE].